

Fabrication and Visible-Light Photocatalytic Performance of Two-Dimensional ZnO/Bi_{3.9}Zn_{0.4}V_{1.7}O_{10.5} Nanoscale Heterostructures

Mao Tingjie, Ye Shengbing, Luo Qingfeng, Chen Yangguang, Fang Xutao, Hu Te, Tong Yanhua

Huzhou University, Huzhou 313000, China

Abstract: Two-dimensional (2D) ZnO/Bi_{3.9}Zn_{0.4}V_{1.7}O_{10.5} nanosheets were prepared using Zn₅(CO₃)₂(OH)₆ nanosheets as substrate to anchor BiVO₄ followed by calcination. As-prepared samples were characterized by X-ray diffraction and transmission electron microscopy with elemental mapping attachment. Results show that with the increasing Zn/Bi molar ratio, the surface composition of ZnO porous nanosheets evolves into Bi_{3.9}Zn_{0.4}V_{1.7}O_{10.5} step by step. When the Zn/Bi molar ratio is above 1:0.02, additional BiVO₄ begins to form and grows into particles in the Bi_{3.9}Zn_{0.4}V_{1.7}O_{10.5} region. Diffuse reflectance spectra of as-prepared samples reveal that nanoscale heterostructures harvest visible light of 400–600 nm dependent on the varying Zn/Bi molar ratio. The experiment for photocatalytic degradation of rhodamine B under visible light ($\lambda \geq 420$ nm) illumination shows that the 2D heterostructure with the Zn/Bi molar ratio of 1:0.0133 performs the best photocatalytic activity in spite of no remarkable visible-light absorption. Photoluminescence and photoelectrochemical tests indicate that the enhancement in catalytic activity is attributable to an effective separation and transfer of photoinduced carriers caused by the ZnO/Bi_{3.9}Zn_{0.4}V_{1.7}O_{10.5} heterostructure. The 2D surface heterogenization can promote the photocatalytic process, being applicable to a wide range of 2D nanostructures.

Key words: Bi_{3.9}Zn_{0.4}V_{1.7}O_{10.5}; nanosheets; visible light; photocatalyst

Semiconductor photocatalysis is a promising approach for environmental detoxification^[1-3], which is capable of converting toxic and nonbiodegradable organic compounds into carbon dioxide and inorganic constituents. Among various semiconductors applied, titanium dioxide (TiO₂) and zinc oxide (ZnO) are most widely employed for photocatalysts due to their high activity to remove a wide range of organic pollutants from air and water. Compared with TiO₂, ZnO is a sort of bio-safe and biocompatible material with low cost and easy synthesis^[4]. Besides, ZnO basically exhibits better electron transfer and more efficiency than TiO₂ in photocatalytic degradation of some dyes under visible light illumination^[5-7]. In this regard, ZnO could become a promising photocatalyst for application.

However, pristine ZnO has high recombination rate of photo-generated carriers, directly causing low photochemical converting efficiency. Combining with another semiconductor to construct a heterojunction is prevalently employed to solve the above-mentioned issue. Up to now, a lot of ZnO-based semiconductors were fabricated and their photocatalytic activities were enhanced in varying degrees, including TiO₂^[8], BiOBr^[9] and AgCl^[10]. Besides, large band gap of ZnO (~3.3 eV) allows it to only absorb UV light occupying 5% of solar spectrum, which leads to a low photodegradation efficiency under solar irradiation. Several strategies have been adopted to extend spectral response of ZnO, such as doping with nonmetal (C, N, S)^[11-13], metal (Cu, Cr, Ce, La)^[14-16], and sensitization. Among them, sensitization using visible-light

Received date: May 5, 2019

Foundation item: National Natural Science Foundation of China (21607041); Science and Technology Planning Project of Zhejiang Province, China (2017C33240); Undergraduate Student's Research Project on Training Innovation and Enterprise, Qiuzhen School of Huzhou Teachers College (163)

Corresponding author: Tong Yanhua, Ph. D., Associate Professor, Department of Materials and Chemistry, Huzhou University, Huzhou 313000, P. R. China, Tel: 0086-572-2320685, E-mail: yh_tong123@126.com

Copyright © 2020, Northwest Institute for Nonferrous Metal Research. Published by Science Press. All rights reserved.

active materials (for instance, narrow band gap) has been extensively investigated as an effective means not only to improve the harvest of visible light but also to inhibit the recombination of photoinduced carriers.

Bismuth vanadate (BiVO_4) as a visible-light-sensitizing semiconductor has attracted great research interest, owing to narrow bandgap energy (2.45 eV), low cost, chemical and thermal stability and environmentally benign properties^[17]. Singh et al^[18] reported that BiVO_4 -ZnO nanocomposite was synthesized by hydrothermal method followed by annealing at 450 °C and performed 4.3-fold-enhanced photocatalytic activity under sun irradiation with respect to bare ZnO. Fu et al^[19] presented a simple wet-chemical process to obtain ZnO-loaded BiVO_4 spherical-like nanoparticles which irradiated by visible light showed a two-fold enhancement of photocatalytic activity in comparison with unloaded BiVO_4 nanoparticles. Besides, N-doped ZnO nanosheets coupled with BiVO_4 and BiVO_4 /ZnO coupling nanosheet arrays on a conductive magnetically driven cilia film also exhibited much higher visible-light-driven activity for degradation than BiVO_4 alone^[20,21]. The improved visible-light catalytic activity of these BiVO_4 /ZnO heterostructures was ascribed to the formation of intermediate band and comparatively low recombination rate, which facilitates the separation of electron-hole pairs^[18].

However, reported BiVO_4 /ZnO heterostructures were fabricated by annealing of mechanically mixed BiVO_4 and ZnO. There were scarce investigations regarding to using ZnO precursors to prepare BiVO_4 /ZnO heterostructure. In the present work, 2D $\text{ZnO/Bi}_{3.9}\text{Zn}_{0.4}\text{V}_{1.7}\text{O}_{10.5}$ nanoscale heterostructures were prepared using $\text{Zn}_5(\text{CO}_3)_2(\text{OH})_6$ nanosheets as ZnO precursor to anchor BiVO_4 followed by calcination. With the increasing Zn/Bi molar ratio, the harvest of visible light for this modification was gradually enhanced. However, modified ZnO nanosheets with the Zn/Bi molar ratio of 1:0.0133 exhibited the best visible-light-driven photocatalytic degradation efficiency, although it did not have a remarkable absorption in visible-light region. Characterization of photoluminescence, photocurrent and electrochemical impedance demonstrated that the enhanced photocatalytic activity compared with single-component counterparts was mainly ascribed to good separation and transfer of photoinduced carriers.

1 Experiment

All major chemicals of analytical grade were purchased from Aladdin Reagent Co. Ltd, Shanghai China and used as received without further purification. All the solutions were prepared with doubly distilled water.

$\text{Zn}_5(\text{CO}_3)_2(\text{OH})_6$ (ZCH) nanosheets were prepared by a hydrothermal approach similar to our reported procedures^[22]. $\text{Zn}(\text{CH}_3\text{COO})_2 \cdot 2\text{H}_2\text{O}$ (0.23 g) was dissolved in distilled water (75 mL), followed by adding urea (0.29 g) and hexadecyl trimethyl ammonium bromide (0.047 g). The resulting mixture

was magnetically stirred for 1 h to form transparent solution and then transferred into a Teflon-lined autoclave of 100 mL. The autoclave was then screwed up and kept inside an electric oven at 80 °C for 4 h and 120 °C for 3 h. After cooling to room temperature naturally, cotton-like suspended solid was collected by centrifugation and then washed with deionized water and absolute ethanol several times.

$\text{ZnO/Bi}_{3.9}\text{Zn}_{0.4}\text{V}_{1.7}\text{O}_{10.5}$ (ZnO/BZVO) heterostructures were prepared by a precursor-deposited method in combination with calcination. A typical procedure was as follows. A whole portion of prepared ZCH nanosheets were put into 100 mL distilled water and dispersed by sonicating. Then, a calculated amount of Na_3VO_4 was added in the above-mentioned mixture and dissolved under magnetic stirring. This system was vigorously stirred for 30 min so that part of VO_4^{3-} ions could be adsorbed on the surface of ZCH nanosheets by electrostatic interaction. Subsequently, a required amount of $\text{Bi}(\text{NO}_3)_3 \cdot 5\text{H}_2\text{O}$ dissolved in ethylene glycol was dropwise added to the above-made mixture, the amount of which was varied to obtain serial samples with varying molar ratio of Zn to Bi (1:0.0033, 1:0.0067, 1:0.0133, 1:0.02, 1:0.04, 1:0.067, 1:0.2). The above-mentioned whole process was carried out at room temperature under magnetic stirring. The resulting ZCH- BiVO_4 combined samples were centrifuged, washed thoroughly with distilled water, and then dried at 65 °C for 12 h.

BiVO_4 -modifying ZnO nanosheets were obtained after calcining a series of ZCH- BiVO_4 combined samples at 500 °C for 2 h. For comparison, pristine BiVO_4 was prepared by the same process without ZCH nanosheets. The as-prepared samples with the Zn/Bi molar ratio of 1:0.0033, 1:0.0067, 1:0.0133, 1:0.02, 1:0.04, 1:0.067, 1:0.2 were denoted as ZB_0.0033, ZB_0.0067, ZB_0.0133, ZB_0.02, ZB_0.04, ZB_0.067, ZB_0.2, respectively.

The phase composition and crystal structure of as-fabricated samples were determined by powder X-ray diffraction (XRD, XD-6 with $\text{Cu K}\alpha$ radiation at a scan rate of 0.02°s^{-1}). The morphology and elemental mapping of the samples were studied by transmission electron microscopy (FEI-Tecna F20) at an accelerating voltage of 200 kV. UV-vis diffuse reflectance spectra (DRS) were measured using a UV-vis spectrophotometer (EVOLUTION 220) with an integrating sphere under ambient conditions. Photoluminescence (PL) spectra were tested on a fluorescence spectrophotometer (fluoroSENS-9000, UK) equipped with a filter ($\lambda < 360$ nm) at an export of the excitation channel and another filter ($\lambda > 380$ nm) at an entry of the emission channel. The photoelectric current (PC) and electrochemical impedance spectroscopy (EIS) of the photocatalyst were recorded through a CHI760E A17122 electrochemical workstation (Ivium CompactStat. h., Netherland).

The photocatalytic experiment was carried out as our previous report^[22]. Rhodamine B (RhB) was chosen as a photo-degradation object. Glass beakers (capacity ca. 100 mL)

were used as photoreactor vessels. The reaction system containing RhB (3 mg/L, 20 mL) with a pH of 6.56 and photocatalysts (10 mg) was sonicated for dispersion and stirred in the darkness for 15 min to reach an adsorption equilibrium of RhB on the surface of photocatalysts. Afterwards, it was placed into cylinder-shaped tank filled with circulating water and irradiated by visible light under magnetic stirring for a given period. The visible light with wavelength ranging from 420 nm to 750 nm was produced from a 300 W Xenon lamp (Model CEL-HXF300) with a UVIRCUT 420 filter. After the photocatalytic reaction, degradation suspensions under different illumination periods were centrifuged to separate the photocatalysts. The absorption spectra of RhB solutions under different photocatalytic periods were estimated using a UV-vis spectrophotometer (Shimadzu UV 2600). The absorption peak at 553 nm represents the aromatic content of RhB and its decrease indicates the degradation of dye. The stability of the photocatalysts was obtained through three successive cycling experiments. After each run, photocatalyst powder were collected though washing with deionized water and absolute ethanol several times, separately, to remove the remained RhB and/or degradation products.

2 Results and Discussion

2.1 Phase structure and morphology of as-prepared samples

Fig.1a shows XRD patterns of modified ZnO samples with varying Zn/Bi molar ratios along with bare ZnO and BiVO₄ for comparison. All the diffraction peaks of pristine ZnO (pattern a) in Fig.1a were perfectly assigned as the hexagonal phase of ZnO, coinciding well with the standard data of ZnO (JCPDS card 36-1451). Most diffraction peaks of pristine BiVO₄ are consistent with the tetragonal phase of BiVO₄ (JCPDS card 14-0688), as shown in pattern i in Fig.1a. In the XRD patterns of modified-ZnO samples (patterns b~h in Fig.1a), with an increasing Zn/Bi molar ratio, a new diffraction peak at 28.5° begins to form at 1:0.0133 and then be gradually intensified. This diffraction peak denoted as solid inverted triangle symbol along with other new diffraction peaks could be indexed to the tetragonal BZVO phase (JCPDS No. 48-0276). Upon the Zn/Bi molar ratio increasing to 1:0.2, another new phase of BiVO₄ (marked as hollow inverted triangle symbols) yields in the ZnO/BZVO heterostructures. These results suggest that under low content of deposited BiVO₄, BiVO₄ can completely react with surface of ZCH substrate at 500 °C to produce BZVO. While the quantity of deposited BiVO₄ reaches a certain value, some part of BiVO₄ far from the surface of ZCH could not participate in reaction and be left. Accordingly, as the Zn/Bi molar ratio increases, BZVO first yield and then grow. When the ratio is enough high, formation of BiVO₄ on the surface of BZVO region would occur.

It is observed that all of hexagonal ZnO diffraction peaks

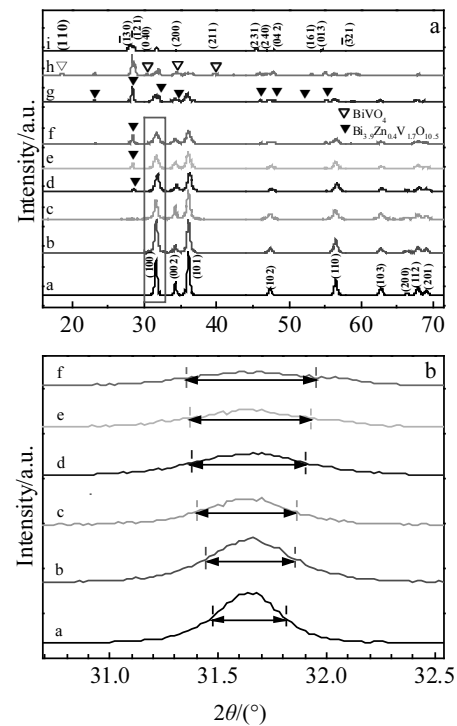


Fig.1 XRD patterns of as-prepared samples (a): a-ZnO, b-ZB_0.0033, c-ZB_0.0067, d-ZB_0.0133, e-ZB_0.02, f-ZB_0.04, g-ZB_0.067, h-ZB_0.2, i-BiVO₄; (b) enlarged (100) diffraction peaks of ZnO in modified samples with the increasing Zn/Bi molar ratio

for modified-ZnO samples are gradually weakened with the increasing Zn/Bi molar ratio. Furthermore, the diffraction peaks of (100) at 31.65° of ZnO phase, magnified in Fig.1b, illustrate the increasing width at half-peak height with the increase of Zn/Bi molar ratio. The weakening and broadening of ZnO diffraction peaks in composite compared with the bare ZnO demonstrates a decrease in size of ZnO in composite. This is because the production of BZVO sacrifices part of ZnO precursor. This in-situ growth could endow ZnO/BZVO nanoscale heterostructure with a strongly bound interface between BZVO phase and ZnO substrate.

As displayed in Fig.2, surface morphology of porous nano-sheets evolves with the increasing Zn/Bi molar ratio. Pristine ZnO is porous sheetlike morphology (Fig.2a), the surface of which is smooth. At the molar ratio of 1:0.0067 of Zn to Bi, brightness contrast and roughness are observed on a porous nanosheet (Fig.2b). The dark region on the porous sheet would be BZVO. When the Zn/Bi molar ratio increases to 1:0.02, dark region overspreads large part of porous nanosheets. Besides, few particles grow on the surface of nanosheets. Upon the Zn/Bi molar ratio reaching 1:0.067, more and larger particles are observed on the surface of porous nanosheets. This morphology evolution with the increasing Zn/Bi molar ratio in combination with the XRD characterization results

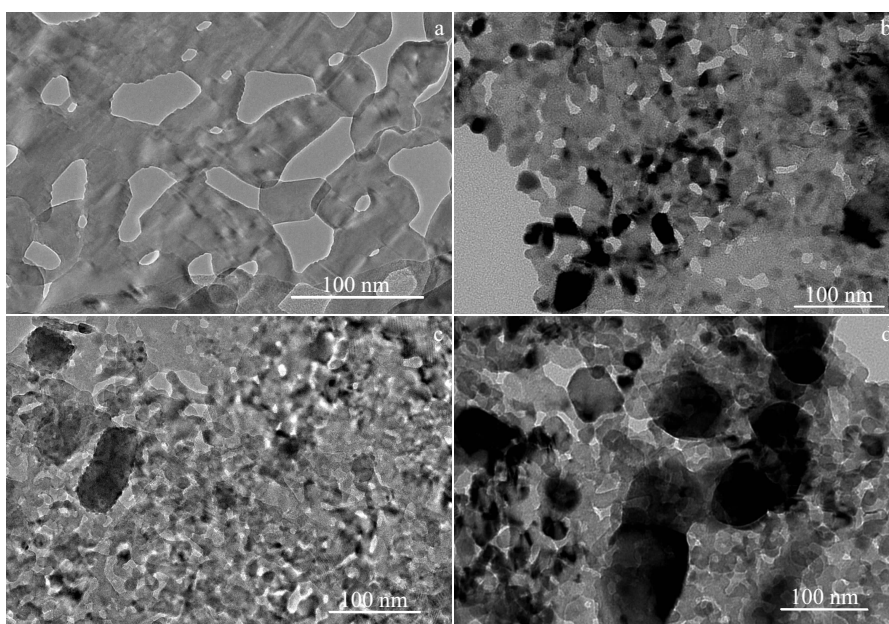


Fig.2 TEM images of as-prepared samples with varying Zn/Bi ratios: (a) 1:0, (b) 1:0.0067, (c) 1:0.02, and (d) 1:0.067

demonstrates that the dark region is BZVO and particles are BiVO_4 .

To further corroborate this derived result, elemental mapping for ZB_0.067 was measured considering that the Bi content in ZB_0.0133 was possibly lower than the element-detecting limit of EDS. Their element mapping images are shown in Fig.3. The mapping signals of Zn and O elements are more intensive than those of Bi and V elements, indicating that ZnO is the main chemical composition of nanosheets.

Mapping images of Bi and V elements display that they are homogeneously distributed in nanosheets. Only the image of Zn elemental mapping does not show loaded-particle shapes, suggesting the substance of the loaded particles is BiVO_4 . As a result, with the increasing Zn/Bi ratio, surface of ZnO porous nanosheets gradually changes into BZVO. While the Zn/Bi ratio ≥ 0.02 , additional BiVO_4 particles grow on the surface of BZVO region.

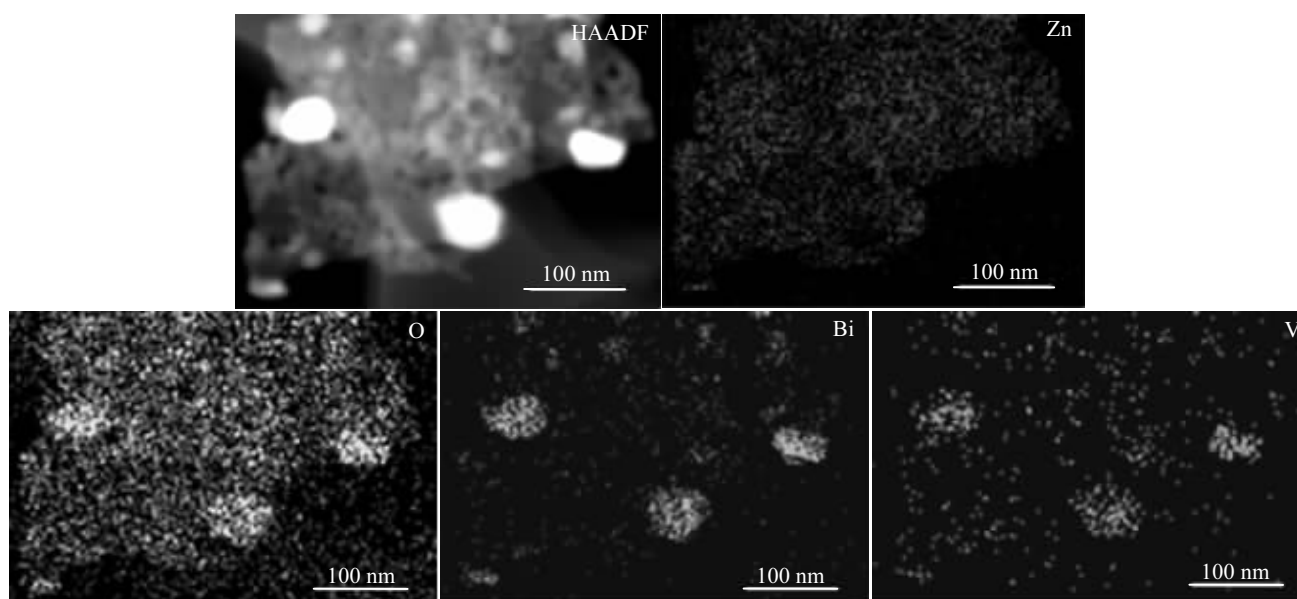


Fig.3 TEM elemental mapping images of BiVO_4 -modifying ZnO sample with the Zn/Bi ratio of 1:0.067

2.2 Formation mechanism of ZnO/BZVO porous nanosheets

Based on the above results, we proposed a formation mechanism for 2D ZnO/BZVO nanoscale heterostructures (Fig.4). Typically, the surface of as-prepared ZCH nanosheets with partial deficiency of CO_3^{2-} groups presents electropositivity^[23] and is easily anchored by VO_4^{3-} anions. When low content of VO_4^{3-} anions was added into aqueous solution containing dispersed ZCH nanosheets, all VO_4^{3-} anions could be adsorbed on the surface of ZCH nanosheets (Eq. (1)). Upon the addition of Bi^{3+} ions, they would react with anchored VO_4^{3-} anions to produce BiVO_4 on the surface of ZCH nanosheets (Eq. (2)). At 500 °C for 2 h, the low-content anchored BiVO_4 would completely react with its contact part of ZCH nanosheets to produce $\text{Bi}_{3.9}\text{Zn}_{0.4}\text{V}_{1.7}\text{O}_{10.5}$ (Eq. (3)) and other ZCH evolved into ZnO. Owing to the evolution of CO_2 and H_2O gas from the pyrolysis of ZCH, nanosheets turned into porous nanosheets (Fig.4I). At high levels of VO_4^{3-} anions, only part of VO_4^{3-} anions could be adsorbed on the surface of ZCH nanosheets due to saturation, leaving free VO_4^{3-} anions in mixed solution. Subsequently, Bi^{3+} ions at the equal amount of VO_4^{3-} dissolved in ethylene glycol was drop by drop added into the above system. Bi^{3+} ions would firstly combine with the anchored VO_4^{3-} anions to yield BiVO_4 nuclei and next these nuclei grew up under free VO_4^{3-} anions in the solution and Bi^{3+} ions from continuous addition. These composite with high content of BiVO_4 were calcined at 500 °C; part of BiVO_4 reacted with the contact part of ZCH to produce $\text{Bi}_{3.9}\text{Zn}_{0.4}\text{V}_{1.7}\text{O}_{10.5}$ and left BiVO_4 were crystallized into particles (Eq. (4)) on the surface of $\text{Bi}_{3.9}\text{Zn}_{0.4}\text{V}_{1.7}\text{O}_{10.5}$ (Fig.4II).

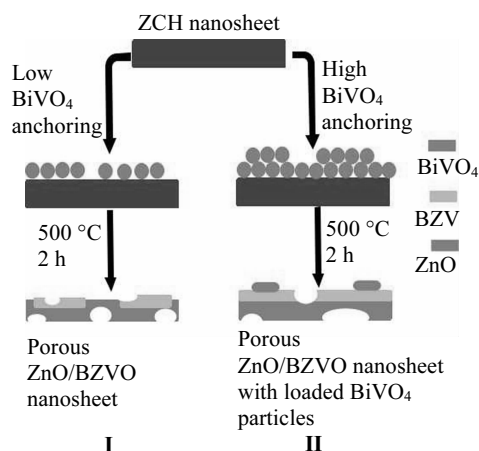
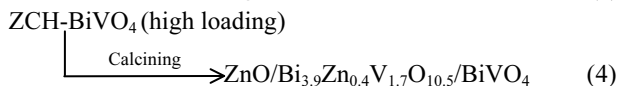
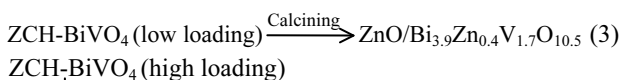


Fig.4 Schematic representation of the formation mechanism of BiVO_4 -modifying ZnO nanostructures under different conditions of anchoring

2.3 Optical absorption and PL properties

UV-vis diffuse reflectance spectra of as-prepared samples are presented in Fig.5. For ZnO and BiVO_4 , the absorption band edges are roughly at 420 and 610 nm, respectively. It indicates that ZnO only absorbs UV light, and BiVO_4 has a strong absorption in the visible-light range from 400 nm to 500 nm. With respect to ZnO, visible light in the region of 400~550 nm for BiVO_4 -modifying ZnO nanosheets are gradually harvested with the increasing content of Bi. This can be further proved by photos of as-prepared samples shown in Fig.6, which displays that the color is gradually deepened from white to orange with the increasing Bi content. Harvesting the visible component of solar radiation for BiVO_4 -modifying ZnO nanosheets is expected to enhance visible-light-driven photocatalytic efficiency.

The PL spectra of selected samples are shown in Fig.7 for the purpose of investigating the migration and transfer behaviors of photoinduced e^-/h^+ . ZnO, ZB_0.0033, ZB_0.0133 and ZB_0.067 display three main emissions excited by an excitation wavelength of 330 nm at room temperature. The ultraviolet emission band centered at approximately 375 nm is due to the radiative exciton recombination. A violet shoulder on the lower-energy at around 400 nm should be assigned to the transition from interstitial zinc to valence band^[24]. The visible emission observed over the wide range of 500~800 nm is attributed to the deep level emission of interstitial oxygen and antisite oxygen (O_{Zn}) defect states in the crystal structure of ZnO^[24,25] for pure BiVO_4 does not exhibit emission. With the increasing Zn/Bi molar ratio, the intensity of these emission peaks gradually decreases to the minimum at 1:0.0133 followed by an increase. It indicates that only a small quantity of BZVO modification can facilitate the migration and transfer of photoexcited e^-/h^+ pairs on ZnO nanosheets and thus is expected to enhance photocatalytic activity.

2.4 Photoelectrochemical properties

The separation efficiency of charge carriers for as-prepared pristine ZnO, BiVO_4 and BZVO-modified ZnO heterostructures was determined by PC and EIS experiments. Fig.8a shows current-time curves for the as-prepared sample under intermit-

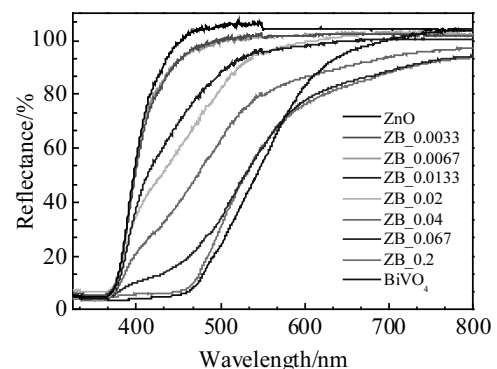


Fig.5 UV-visible diffuse reflectance spectra of as-prepared products



Fig.6 Photos of as-prepared products: (a) ZnO, (b) ZB_0.0033, (c) ZB_0.0067, (d) ZB_0.0133, (e) ZB_0.02, (f) ZB_0.04, (g) ZB_0.067, (h) ZB_0.2, and (i) BiVO₄

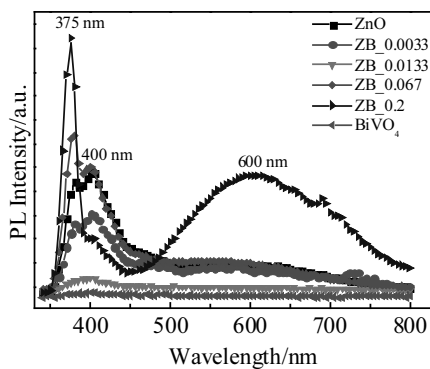


Fig.7 Photoluminescence emission spectra of ZnO, ZB_0.0033, ZB_0.0133, ZB_0.067, ZB_0.2 and BiVO₄ excited by light with wavelength at 330 nm at room temperature

tent visible light ($\lambda > 420$ nm). Only BiVO₄ electrode generates cathode photocurrent suggesting p-type semiconducting property, while ZnO and BZVO-modified ZnO exhibit anode photocurrent response reflecting n-type semiconductor. As shown in Fig.8a, with the increasing Zn/Bi molar ratio, the photocurrent density of BZVO-modified ZnO increases to the maximum at the molar ratio of 1:0.0133 and then decreases, compared with pristine ZnO. This phenomenon demonstrates that BZVO/ZnO heterostructure with low BZVO content can promote the separation of photogenerated carriers. Although pure BiVO₄ performs the best photocurrent at the moment of opening light, it quickly drops as the irradiation time prolongs. To investigate the mobility of photoexcited carriers, EIS of as-synthesized samples was further measured in the dark, and the EIS Nyquist plots are displayed in Fig.8b. The diameter of

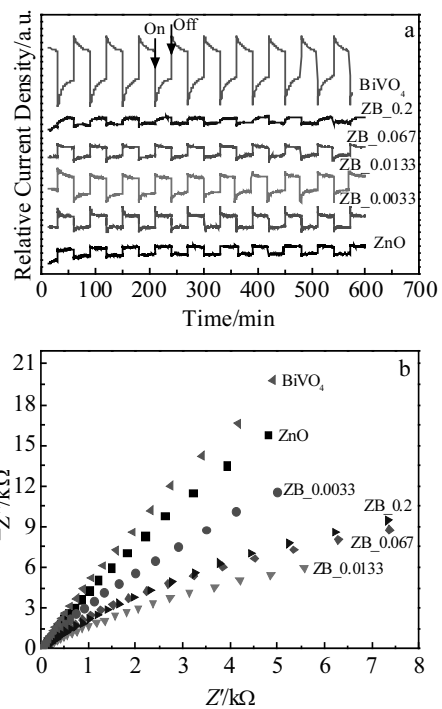


Fig.8 Transient photocurrent density with light on/off cycles under visible light irradiation (a) and EIS Nyquist plots of ZnO, ZB_0.0033, ZB_0.0133, ZB_0.067, ZB_0.2 and BiVO₄ electrodes measured in mixed phosphate solution with pH of 6.86 (b)

the semicircle of the EIS Nyquist plots is directly related to the transfer efficiency of carriers, and the smaller radius reflects higher separation efficiency. In terms of pristine ZnO

and BiVO_4 , a relatively smaller arc radius is found for BZVO-modified ZnO. Among them, ZB_0.0133 heterostructure performs the smallest arc radius, which is evidence of high mobility of carriers.

2.5 Photocatalytic behavior of ZnO/BZVO nanosheets

The degradation of RhB was used for assessing the visible-light-driven photocatalytic activity of the as-prepared nanoscale samples. Photocatalytic degradation experiment for each sample was parallelly carried out three times to prevent abnormal data. Fig.9 shows the variation of relative average concentration of RhB dependent on visible-light irradiation time with error bars for the as-prepared samples. Without photocatalysts, no remarkable degradation is observed, suggesting that self-degradation of RhB is difficult to occur. Although pristine ZnO porous nanosheets do not have absorption in visible-light region, it still performs photocatalytic activity under visible-light irradiation. This is perhaps because the UVIRCUT 420 filter does not completely cut off UV light and a little bit of them can penetrate through the filter. In Fig.9, it is observed that the BZVO-modified ZnO nanosheets perform enhanced catalytic activity compared with their single-composition counterparts, except for samples with ZnO/Bi molar ratio of 1:0.0033 and 1:0.2 whose catalytic activity is near to that of pristine ZnO and BiVO_4 . Among these samples, ZB_0.0133 exhibits the highest catalytic efficiency, which is around two times higher than ZnO (ZnO takes 105 min to degrade 69% of RhB; ZB_0.0133 takes 45 min to degrade 68% of RhB).

Fig.10 shows a temporal evolution of UV-Vis absorption spectrum of RhB solution with ZB_0.0133 as irradiation time prolongs up to 105 min. It is observed that RhB shows a major absorption band at about 553 nm. As the irradiation time prolongs, the RhB absorption decreases rapidly and the maximum absorption weak shifts from 553 nm to 496 nm. Meanwhile, it is found that the color of the suspension also changes from initial fuchsia to light-colored, suggesting that the ZB_0.0133 exhibits good catalytic activity for RhB degradation under visible light conditions.

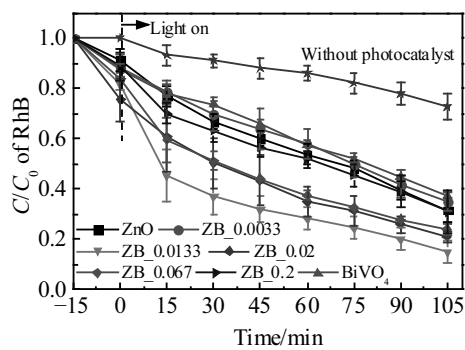


Fig.9 Variation of the relative content of RhB (C/C_0) in the darkness and then under visible light irradiation ($\lambda \geq 420$ nm) in the absence/presence of photocatalysts

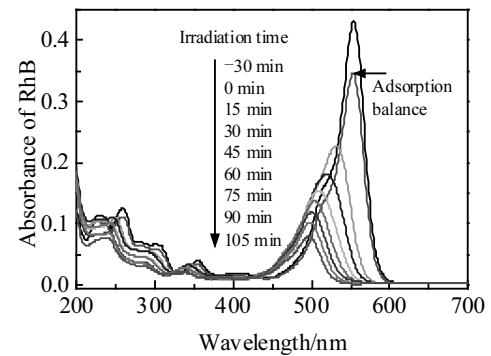


Fig.10 Temporal UV-vis absorption spectral variations of RhB aqueous solution with prolonged irradiation time

Apart from good catalytic activity, the recyclability of any photocatalyst has a very important effect on its practical application. Thus, the recycling degradation experiments were carried out to test the stability of the ZB_0.0133 and the corresponding curves are shown in Fig.11. After three recycles, the ZB_0.0133 photocatalyst still performs good degradation efficiency of 80%, which is 95.2% of the corresponding fresh catalyst. All XRD peaks of BZVO-modified ZnO nanosheets after three successive recycles can be assigned to tetragonal BZVO and hexagonal ZnO (Fig.12) in accord with the composition of the fresh sample, although the diffraction intensity of the recycled sample is weaker than that of the fresh one possibly due to undergoing a dissolution-precipitation process in each washing cycle. It represents that BZVO-modified ZnO nanosheets have tolerable stability and no serious photocorrosion during the washing and recycling process.

2.6 Discussion of enhanced photocatalytic mechanism

Photocatalytic activity has many influencing factors including light response, specific surface area, energy levels (valence-band maximum (VBM) and conduction-band minimum (CBM))

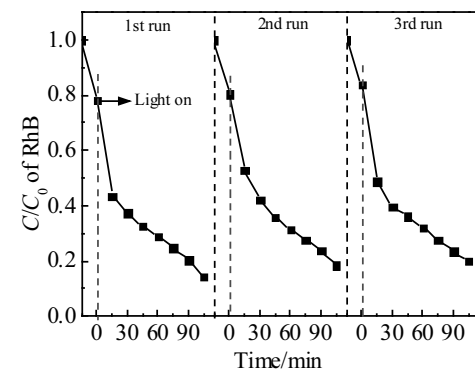


Fig.11 Cycling runs in the adsorption and degradation of RhB over the ZB_0.0133 under visible light illumination

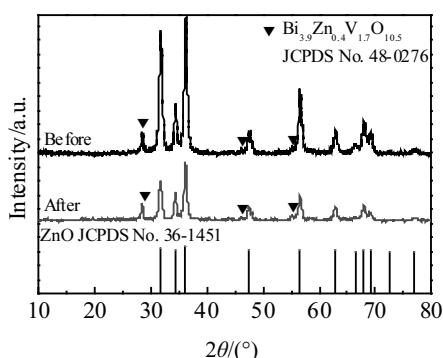


Fig.12 XRD patterns of the BZ_0.0133 before and after three cycles

and separation and migration of photogenerated carriers. Since TEM images show that BZVO modification on the surface of ZnO nanosheets does not change the sheetlike morphology, the effect from specific surface area can be ruled out. Although the increasing BZVO content raises the band gap of ZnO phase leading to higher VBM and lower CBM energy levels, BZVO is the main visible-light-response composition in the BZVO-modified ZnO heterostructure. So, energy levels can also be ruled out. In terms of our BZVO-modified ZnO heterostructure, the enhanced photocatalytic activity has to be ascribed to the separation and migration of photoinduced carriers.

Based on the measurement results of PL and PC, a possible mechanism for enhanced photocatalytic activity for as-prepared composite samples was discussed. At low level of BZVO, the thickness of ZnO nanosheets have little variations and a type-II heterostructure forms between wide band-gap ZnO and narrow band-gap BZVO, whose band alignment is schematically illustrated in Fig.13 (left). The position of CB and VB of ZnO is both lower than that of BZVO, which could promote the photoexcited electrons and holes to facilitate transfer in opposite directions and subsequently result in an efficient spatial separation.

However, the thickness of ZnO nanosheets becomes thinner and thinner with the increasing BZVO content, which could

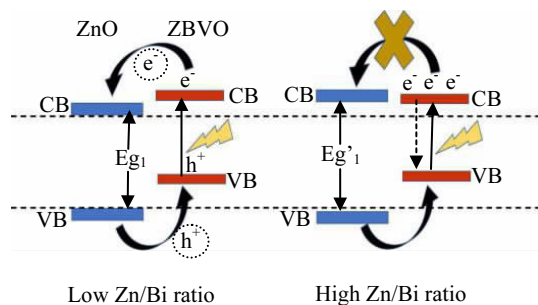


Fig.13 Schematic of band gap alignment of ZnO/BZVO heterostructures with low and high Zn/Bi molar ratio

cause broadening of band gap of ZnO nanosheets due to quantum size effect. The broadening of band gap would give rise to the up-shift of CBM energy level and the down-shift of VBM energy level. Upon the BZVO content being above some value, the CBM energy level could move up higher than that of BZVO, schematized in Fig.13 (right). In this case, photoexcited electrons of BZVO side cannot move to ZnO and some accumulated electrons would combine with photoexcited holes. This would be the reason for a reduction in PC and an increase in PL for ZnO/BZVO with high Zn/Bi ratio although it harvests more visible light. Accordingly, the enhancement in photocatalytic activity for ZnO nanosheets with low-level BZVO modification has to be mainly attributable to the effective separation of photoinduced carriers.

3 Conclusions

1) 2D ZnO/BZVO nanoscale heterostructures are obtained by an integrated route, with hydrothermal, precipitation and thermal-decomposition means being employed.

2) At the Zn/Bi molar ratio of 1:0.0133, BZVO-modified ZnO nanosheets perform the best catalytic efficiency under visible light irradiation in spite of weak visible-light harvest.

3) The separation and transfer of photoinduced carriers play the major role in enhancing photocatalytic activity relative to pristine ZnO. Low-content modification on the surface of two-dimensional nanomaterials could improve photocatalytic activity. The used method is general and applicable to a wide range of similar surface engineering for photocatalytic application.

References

- Hoffmann M R, Martin S T, Choi W *et al.* *Chemical Reviews*[J], 1995, 95(1): 69
- Ghosh S, Kouame N A, Ramos L *et al.* *Nature Materials*[J], 2015, 14(5): 505
- Zhang Yiyang, Gu Di, Wang Baohui. *Rare Metal Materials and Engineering*[J], 2018, 47(11): 3542
- Gu X Q, Li C Y, Yuan S *et al.* *Nanotechnology*[J], 2016, 27: 402001
- Chen L C, Tu Y J, Wang Y S *et al.* *Journal of Photochemistry & Photobiology A: Chemistry*[J], 2008, 199(2): 170
- Ashokrao B P, Kashinath R P, Satish K P *et al.* *Journal of Hazardous Materials*[J], 2010, 183(1): 315
- Kumar S G, Rao K S R K. *RSC Advances*[J], 2015, 5(5): 3306
- Pan L, Shen G Q, Zhang J W *et al.* *Industrial & Engineering Chemistry Research*[J], 2015, 54 (29): 7226
- Yi S S, Zhao F, Yue X Z. *New Journal of Chemistry*[J], 2015, 39(8): 6659
- Phuruangrat A, Oncharoen T, Ekthammathat N *et al.* *Russian Journal of Physical Chemistry A*[J], 2019, 93(2): 319
- Kumari V, Mittal A, Jindal J. *Frontiers of Materials Science*[J], 2019, 13(1): 1
- Su Y P, Li S, He D S *et al.* *Journal of Alloys and Compounds*[J],

- 2018, 6(9): 11989
- 13 Farhadian N, Akbarzadeh R, Pirsahab M et al. *International Journal of Biological Macromolecules*[J], 2019, 132: 360
- 14 Jiang J J, Mu Z, Xing H M et al. *Applied Surface Science*[J], 2019, 478: 1037
- 15 Meng A, Xing J, Li, X J et al. *Journal of Nanoscience and Nanotechnology*[J], 2019, 19(5): 2617
- 16 Sheydaei M, Ghalamchi L, Vatanpour V. *Ultrasonics Sonochemistry*[J], 2019, 56: 361
- 17 Tan H L, Amal R, Ng Y H. *Journal of Materials Chemistry A*[J], 2017, 5: 16498
- 18 Singh S, Sharma R, Joshi G et al. *Korean Journal of Chemical Engineering*[J], 2017, 34(2): 500
- 19 Fu X D, Xie M Z, Luan P et al. *ACS Applied Materials & Interfaces*[J] 2014, 6(21): 18550
- 20 Singh S, Sharma R, Mehta B R. *Applied Surface Science*[J], 2017, 411: 321
- 21 Peng F P, Ni Y R, Zhou Q et al. *Journal of Alloys and Compounds*[J], 2017, 690: 953
- 22 Tong Y H, Zheng C, Lang W J et al. *Materials and Design*[J], 2017, 122: 90
- 23 Ghose S. *Acta Crystallographica*[J], 1964, 17(8): 1051
- 24 Zeng H B, Duan G T, Li Y et al. *Advanced Functional Materials*[J], 2010, 20(4): 561
- 25 Demel J, Pleštil J, Bezdicka P et al. *Journal of Physical Chemistry C*[J], 2011, 115(50): 24702

二维 ZnO/Bi_{3.9}Zn_{0.4}V_{1.7}O_{10.5} 纳米异质结构的制备及其可见光催化活性

毛挺杰, 叶圣炳, 罗青丰, 陈阳光, 方徐涛, 胡特, 童艳花

(湖州师范学院, 浙江 湖州 313000)

摘要: 利用 Zn₅(CO₃)₂(OH)₆ 纳米片为基底沉积了 BiVO₄ 再通过煅烧成功制备了二维 ZnO/Bi_{3.9}Zn_{0.4}V_{1.7}O_{10.5} 复合纳米片。通过 X 射线衍射, 透射电镜和元素映像技术表征了所制样品。结果显示随着锌与铋的原子比的上升, ZnO 多孔片状的表面逐渐变成 Bi_{3.9}Zn_{0.4}V_{1.7}O_{10.5} 物质。但其比例高于 1:0.02 时, 在片状 Bi_{3.9}Zn_{0.4}V_{1.7}O_{10.5} 的区域表面又生长出 BiVO₄ 纳米颗粒。漫反射光谱测试显示出 ZnO/Bi_{3.9}Zn_{0.4}V_{1.7}O_{10.5} 复合物随着锌与铋的原子比的上升其在 400~600 nm 可见光区的吸收逐渐增强。所制样品在可见光(波长大于 420 nm)进行了光催化降解罗丹明 B 的测试, 结果表明在所制样品中, 锌与铋的原子比为 1:0.0133 的 ZnO/Bi_{3.9}Zn_{0.4}V_{1.7}O_{10.5} 纳米片虽然其可见光的吸收并没有明显增强但却表现出最佳的光催化活性。荧光与电化学测试得出了低含量 BZVO 的 ZnO 纳米片可见光催化活性的提高主要是因为表面 ZnO/Bi_{3.9}Zn_{0.4}V_{1.7}O_{10.5} 异质结构提高了光生载流子的分离与传送。这种二维材料的表面建造有利于光催化的进行。因此, 此法可应用于其它二维纳米材料的建造以提高光催化活性。

关键词: Bi_{3.9}Zn_{0.4}V_{1.7}O_{10.5}; 纳米片; 可见光; 光催化剂

作者简介: 毛挺杰, 男, 1997 年生, 湖州师范学院, 浙江 湖州 313000, 电话: 0572-2320685, E-mail: 1009265390@qq.com